*metals*

MDPI

*Article*

# Silicon Effect and Microstructural Evolution of Hot Dip Galvanized Coating of Structural Steels

**Christian Sánchez [1,*], Oscar Bustos [1], Alfredo Artigas [1,2] and Hector Bruna [1,2]**

[1] Departamento de Ingeniería Metalúrgica, Universidad de Santiago de Chile, Santiago 9160000, Chile; oscar.bustos@usach.cl (O.B.); alfredo.artigas@usach.cl (A.A.); hector.bruna@usach.cl (H.B.)
[2] Laboratorio SIMET-USACH, Universidad de Santiago de Chile, Santiago 9170124, Chile
* Correspondence: christian.sanchez@usach.cl

**Abstract:** The microstructure of the coating during hot-dip galvanizing under industrial conditions of two structural steels, a low-silicon ASTM A36 steel and a high-silicon Q345B steel, both of commercial grade, have been characterized for industrial-relevant times. In both cases, it is noted that the formation of the Fe–Zn phases begins in the early stages in the heating step of the steel, a situation in which all the phases are in the solid state. These last observations have been taken into consideration and the microstructures of short times are analyzed, showing that the effect of silicon is present at longer times. The characterization was carried out through traditional metallographic techniques including SEM-EDS and XRD equipment. The evolution in time of the microstructure of both steels is examined, being able to observe that the mechanism by which silicon accelerates the formation of Fe–Zn phases in galvanizing is related to the presence of the liquid phase in contact with the ζ layer formed in earlier times, accumulating silicon in the ζ–liquid interphase. These results are directing the analysis towards proposing the hypothesis of a mechanism of penetration of the liquid phase through ζ–ζ boundaries by variations in the surface free energies that allow the penetration of the liquid phase according to the Gibbs Smith condition. Finally, the observations provided us with a deeper understanding of the phase evolution in the hot-dip galvanizing of high silicon steels.

**Keywords:** hot dip galvanizing; silicon steels; Sandelin; structural steel; corrosion protection; Fe–Zn phases; Gibbs Smith condition

check for updates

**Citation:** Sánchez, C.; Bustos, O.; Artigas, A.; Bruna, H. Silicon Effect and Microstructural Evolution of Hot Dip Galvanized Coating of Structural Steels. *Metals* **2023**, *13*, 1892. https://doi.org/10.3390/met13111892

Academic Editor: Frank Czerwinski

Received: 1 September 2023
Revised: 6 November 2023
Accepted: 10 November 2023
Published: 14 November 2023

**Copyright:** © 2023 by the authors. Licensee MDPI, Basel, Switzerland. This article is an open access article distributed under the terms and conditions of the Creative Commons Attribution (CC BY) license (https://creativecommons.org/licenses/by/4.0/).

## 1. Introduction

The utilization of zinc in various industries has been extensive and significant, with approximately half of the globally produced zinc being designated for protective purposes. Specifically, 50% of the zinc production worldwide is meticulously employed as a protective barrier, acting as an anti-corrosion agent, primarily for steel. This protective mechanism is achieved through a process known as hot-dip galvanizing.

The hot-dip galvanizing process, a method that has been utilized for decades and has been subject to rigorous scientific studies and advancements, involves a series of steps that culminates in the immersion of steel products into a molten bath of zinc. This bath is maintained at a carefully controlled temperature, approximately 450 °C, ensuring optimal adherence and coating properties. The purpose of this process, as documented in numerous metallurgical studies and literature [1], is to impart a robust, durable, and resilient zinc coating onto the steel substrate.

In the vast spectrum of metallurgical applications, the practice of general or batch hot-dip galvanizing stands as a paramount technique that extends its influence across a multitude of industries. This technique plays a particularly indispensable role in areas such as electrical transmission infrastructures, a crucial component for the modern world's electrification and communication. Moreover, it provides a shield for highways and roads, essential arteries for transportation and commerce. Port works, which act as significant

nodes for global trade, similarly benefit from this process. Additionally, airports, those pivotal junctions that facilitate international travel and connectivity, employ galvanized materials to ensure longevity. Not to be overlooked, street furniture, an integral part of urban aesthetics and functionality, and the burgeoning salmon industry, also capitalize on the advantages brought forth by hot-dip galvanizing.

Over the past decade, another noteworthy application has emerged: large-scale mining, a sector that significantly contributes to global resources and economy, has adopted this method to bolster the resilience of its machinery and infrastructure.

Delving into the scientific underpinnings of this technique, one finds that the study of phase transformations in the hot-dip galvanizing process leans heavily on the understanding of the iron–zinc thermodynamic equilibrium. Within this equilibrium, a meticulously sequenced formation of intermetallic compounds is observed. These compounds, exhibiting remarkable stability, grow isothermally in the solid state. Over time, and through extensive research and collaboration, there is now a unanimous consensus in the scientific community regarding the equilibrium of phases that constitute this system, as corroborated by multiple sources [2–5].

Within the comprehensive realm of metallurgical engineering and industrial manufacturing, the hot-dip galvanizing technique stands out as an exemplar of innovation. This technique, refined through years of rigorous research and continuous advancements, hinges on a critical phenomenon-the formation of a robust metallurgical bond between zinc and steel. This is not just any bond, but one that undergoes complex chemical interactions resulting in a meticulously layered protective structure. Each layer in this structure works synergistically, ensuring that the steel beneath is shielded from environmental corrosives, thereby offering an enhanced level of corrosion resistance unparalleled by other surface treatments.

Delving deeper into the intrinsic benefits yielded by this formidable zinc–steel interaction, one discerns the multifaceted advantages it bestows upon the treated products. Foremost among these is the notable extension in the product's operational lifespan. By offering an impregnable shield against corrosion, the steel retains its structural and aesthetic attributes for significantly longer durations. Furthermore, the ancillary benefits are equally compelling. Reduced maintenance costs emerge as a direct consequence of the product's augmented resilience against wear and tear, ensuring that the need for reparative interventions is diminished. This, in turn, translates to increased reliability, a feature that any industry deeply values for its implications on operational continuity and efficiency.

Scaling up our perspective to encompass the broader vista of industrial applications, it becomes abundantly clear that the significance of hot-dip galvanizing transcends its immediate benefits. The technique, in its essence, plays a fundamental and pivotal role in fortifying the backbone of modern infrastructure. Whether we are discussing architecture, transportation networks, or essential utilities, the robustness and integrity of steel-based structures and products are paramount. It is here that hot-dip galvanizing demonstrates its unmatched worth, solidifying its reputation as an indispensable tool in the armory of modern industry.

From a scientific vantage point, the study of phase transformations inherent in the hot-dip galvanizing process provides a fascinating insight into the intricacies of metallurgical interactions. This process is firmly anchored in the principles of the iron–zinc thermodynamic equilibrium. At the heart of this equilibrium lies a meticulous sequence of formation of intermetallic compounds. Remarkably, these compounds exhibit growth isothermally, manifesting their evolution in the solid state, thereby highlighting the depth and complexity of the underlying reactions that define the essence of hot-dip galvanizing.

In the intricate procedure of the galvanizing process, one of the pivotal parameters to be duly noted and monitored is the temperature of the molten zinc bath. Typically, this temperature is maintained around the ballpark figure of 450 °C. At this specified temperature, steel components, meticulously prepared and cleaned prior to immersion, are

submerged into the bath, initiating a complex series of reactions that are integral to the galvanization phenomenon.

Marder [6], through his comprehensive studies and in-depth reviews on the subject, has illuminated the intricate sequence of events that unfold when molten zinc encounters iron under these conditions. He meticulously elaborates that, according to the well-referenced equilibrium diagram, the ensuing formation of layers can be systematically categorized. The initial layer observed is the zinc-saturated alpha iron, which acts as the primary layer of interaction. Following this layer, a cascade of transitions occurs leading to the formation of several distinct layers. These encompass gamma (Γ), followed closely by gamma1 (Γ1), and then, in succession, delta (δ), zeta (ζ), and culminating with the formation of the eta (η) phase. Each of these layers has unique properties and characteristics, playing a vital role in ensuring the integrity and corrosion resistance of the galvanized steel. Multiple studies, as cited [6–8], corroborate these findings and provide further insight into the detailed phase transformation sequence.

Silicon stands as a pivotal element in the realm of steel manufacturing. While it is indispensably required for certain key processes associated with the production of steel, its influence extends far beyond the immediate formation of this alloy. Its consequential effects on the subsequent coating process of steel are pronounced and multifaceted. Depending on its concentration within the steel matrix, silicon can significantly modulate the nature of the coating. This results in variations ranging from extremely thin coatings to notably thick ones. These variances not only alter the visual aesthetics of the coated product but also play a pivotal role in determining its brittleness.

Further diving into the technical intricacies, the interaction dynamics between steel and zinc undergo a profound transformation based on the silicon concentration. There exists a discernible change in the reactivity between the two. Observations suggest that the reactivity reaches its zenith when silicon concentration hovers around the 0.08% mark. Conversely, it dips to its lowest ebb at approximately 0.20% of silicon content. Delving deeper into practical scenarios, it is noteworthy to mention that steel possessing silicon concentrations within the bounds of 0.06–0.13% manifests a substantial increase in the coating thickness. This observation is often referred to as the 'Sandelin Effect', named in tribute to the pioneer who first documented this distinctive silicon-induced phenomenon during the galvanization process back in the 1940s. Moreover, when the silicon concentration surpasses the threshold of 0.3%, the outcome is once again characterized by coatings with elevated thickness, as indicated by numerous studies [9–18].

Up to the present moment, the complex world of metallurgical research has borne witness to the introduction of a multitude of proposed mechanisms. These mechanisms aim to shed light on the intricate processes through which silicon, as a pivotal element, augments and expedites the reactions associated with the galvanization process. Within this vast landscape of theories and hypotheses, a select few have gained considerable traction and recognition in academic circles due to their empirical relevance and profound implications. It is among these prominent theories that the subsequent ones distinctly stand out:

Mackowiak and Short [9], in their meticulously crafted 1979 review, have shed light on the intricate roles various elements play within the sphere of metallurgical reactions, particularly focusing on the pivotal role of silicon. In their elucidation, they articulate the nuanced behavior of silicon in the galvanizing process. Specifically, they highlighted that as the galvanizing duration extends beyond the threshold of 2 min, the dynamic of the reaction experiences a shift. The mode of reaction, initially observed as a parabolic type of attack, undergoes a transformative change, transitioning seamlessly into a linear pattern of response.

This observed phenomenon is not an isolated event but is concomitant with another significant metamorphosis in the process. Namely, the degradation or disintegration of the ζ layer becomes evident, which consequently culminates in the emergence of pronounced, thick individual ζ crystals. Delving deeper into the causative factors underpinning this

behavior, the scholars attribute this specific effect to the intrinsic low-solubility properties of Si when housed within a solid Zn matrix. This solubility characteristic provides a foundation for further postulations. Given the solubility dynamics of Si in solid Zn, it becomes a reasonable supposition to infer that its solubility would also be comparably low within the Fe-Zn compound structures. Building on this premise, it is conceivable that Si predominantly finds itself localized within specific pockets of the liquid Zn phase. These pockets, by virtue of their composition, are strategically situated in the immediate vicinity of the iron surface, thereby playing a potentially crucial role in influencing the galvanizing reaction's overall trajectory.

Kozdras and Nissen, in their detailed 1989 study [10], delved deep into the complexities of the galvanization process, with a specific emphasis on the intricacies surrounding the role of various phases, particularly the Γ phase. In their systematic examination and rigorous analysis, they put forth a meticulously constructed model. This model hinges predominantly on the presence of the Γ phase and its subsequent destabilization during the galvanization sequence. As the reaction progresses and evolves, the δ phase showcases a peculiar behavior: it dissolves a quantum greater amount of silicon compared to other phases. This heightened dissolution behavior essentially means that silicon predominantly finds solace within the δ phase, being stored therein. However, with the subsequent emergence of the ζ phase, an interesting phenomenon occurs. Silicon undergoes a process of segregation, predominantly migrating to the peripheries or edges of the structure. This strategic relocation renders this structure highly vulnerable, making it a prime target for an onslaught by the liquid zinc. As a consequence of this, the layers rich in iron become exposed and are susceptible to aggressive interaction with the molten zinc. The net outcome is the initiation of a highly reactive structure, setting the stage for a series of transformative reactions.

In 1993, Foct [11] proposed a novel mechanism, based on meticulous research and extensive analysis, which elucidates how silicon significantly accelerates the kinetics of galvanizing reactions. In his comprehensive study, he methodically details that when silicon is absent from the system, the ζ phase tends to predominantly nucleate directly upon the steel surface, highlighting a pivotal behavior in the realm of metal chemistry. However, introducing silicon into this equation brings about profound changes at the microscopic level. Specifically, the incorporation of silicon in the system leads to the formation of an exceptionally thin layer of liquid, enriched and saturated with silicon, in immediate proximity to the steel surface. This layer serves as a critical intermediary, facilitating unique reaction pathways. Within this context, the ζ-phase crystals do not nucleate on the iron substrate as one might initially anticipate. Instead, they precipitate slightly beyond the boundaries of the iron substrate. This spatial configuration is intrinsically beneficial, primarily because of the augmented growth it offers, leveraging the remarkable high mobility of iron within this confined, silicon-rich liquid phase. As the crystalline structures of the ζ phase converge and coalesce, the subsequent liquid phase, now in a state of supersaturation with silicon, gives rise to either the δ phase or the complex δ + FeSi mixture, marking the culmination of this intricate reaction sequence.

Guttmann, 1994 [8], in a comprehensive research analysis, articulates a profound understanding of the solubility behaviors in the Fe–Zn system, particularly emphasizing the role of silicon. Due to the exceptionally limited solubility of silicon within the Fe–Zn phases, a distinct reaction pathway ensues. Upon formation of the initial ζ crystals, there is a systematic ejection of silicon atoms, which are subsequently released into the surrounding liquid medium. This expulsion creates a milieu where the liquid becomes significantly enriched in silicon. In this silicon-concentrated liquid phase, which remains trapped and confined between the progressively growing ζ crystals, an immediate and rapid precipitation of FeSi takes place. This reaction is primarily attributed to the fact that the solubility of FeSi within the liquid phase is extremely restricted and minimal. Consequently, this precipitation process effectively desaturates the liquid matrix in terms of its iron (Fe) content. This reduction in iron concentration influences the inherent precipitation behaviors of the Fe–Zn phases. Such dynamics ultimately result in the silicon-rich liquid maintaining its

presence between the ζ crystals. An imperative to understand here is that the solidification temperature of zinc exhibits a decreasing trend as the iron concentration within the system diminishes. This solubility behavior, in turn, facilitates unrestricted access of the liquid phase to the substrate. Such a scenario fosters and promotes the direct dissolution of the substrate, allowing this dissolution process to persistently continue, specifically at the basal regions of the ζ interdendritic spaces, revealing the intricate interplay of solubility and crystal growth in this system.

Marder, 2000 [6], in his meticulously conducted review, provides a comprehensive analysis detailing the nuanced effects on the growth behavior of metallic coatings, particularly emphasizing the influence of silicon (Si). He elucidates that even the presence of seemingly minute concentrations of Si, approximated around a mere 0.1% by weight, can dramatically alter the deposition and growth patterns in galvanizing processes. This alteration is manifested in the form of a transition from the conventionally observed growth pattern to a distinctly linear growth trajectory. Historically, in the absence of silicon, a pure zinc bath would typically exhibit what can be described as a 'uniform attack'. This is predominantly characterized by the sequential and orderly deposition of Fe-Zn alloy layers, indicating a well-structured growth regime. However, with the introduction of the aforementioned small silicon concentrations, this systematic and uniform deposition undergoes a significant transformation. Instead of the classic Fe-Zn alloy layers, the growth behavior starts to manifest in the form of ζ phase crystallites. These newly formed crystallites exhibit unique characteristics and are predominantly encapsulated within a matrix of liquid Zn. Such observations not only underscore the pivotal role played by silicon in influencing and modulating the growth dynamics of metallic coatings, but also highlight the importance of understanding trace element interactions in the realm of materials science and engineering.

Su in 2001 [12], in a comprehensive and methodical assessment of the Fe–Zn–Si system, delves deeply into the intricate relationships and behaviors exhibited within this tri-component system. Throughout his detailed examination, Su meticulously scrutinizes the various mechanisms and theories proposed by different researchers over the years, aiming to elucidate the complex interactions within this system. One of the critical points of his review focuses on a specific mechanism that was earlier proposed by Foct [11]. Foct's hypothesis, which is centered around the δ/liquid equilibrium, garners special attention from Su. After rigorous evaluation and comparative analysis, Su decidedly refutes Foct's proposed mechanism, asserting that its foundational premise concerning the δ/liquid equilibrium does not hold up under rigorous scientific scrutiny. His findings and conclusions, rooted in empirical data and methodical research, suggest that the δ/liquid equilibrium, as conceptualized by Foct, is not as effective or accurate as previously believed. Further cementing Su's position and providing corroborative evidence is the work of another researcher in the field, Raghavan. In 2003 [13], Raghavan's research findings and analyses align with Su's conclusions, verifying the insufficiencies in Foct's proposed mechanism. Raghavan's work, much like Su's, underscores the importance of thorough, evidence-based evaluations in scientific discourse and the continuous quest for accuracy and precision in understanding complex material systems.

In 2016, Sepper [14], drawing upon a rigorous series of tests and evaluations, set forth a comprehensive thesis on the dynamics involved in the galvanization of metallic components. He contends, based on empirical evidence, that throughout the galvanization process, the temperature of the steel consistently ascends, conforming to a discernible heating trajectory. Notably, his investigations reveal a pivotal inflection point: the initiation of galvanizing reactions transpires at a juncture where the temperature resides beneath the threshold melting point of zinc, a circumstance under which every constituent phase remains solid.

Moreover, Sepper's meticulous observations highlight the role of silicon within this context. He discerns that the influence of silicon does not manifest during transient or ephemeral durations. Instead, a profound interplay emerges, centered on the symbiotic relationship between the freshly synthesized protective coating and the prevailing liquid

phase. It is this intricate interaction, he asserts, that culminates in the pronounced hastening of the growth trajectory, a phenomenon pivotal to the understanding of modern galvanization techniques.

The effect of silicon has been faced in the industry using alloy elements in a zinc bath, where the use of nickel stands out. However, nickel is very expensive and other elements have been researched recently.

Bondareva, 2020 [19], investigated the use of nickel tablets to reduce the reactivity of silicon and phosphorus steels during galvanizing. The study found that nickel tablets were effective in reducing the reactivity of all steels tested, with the greatest reduction observed for steels with the highest silicon and phosphorus content. This reduction in reactivity was associated with an improvement in the quality of the zinc coating.

Yu, 2020 [20], delves into the progression of advanced corrosion-resistant coatings for hot-dip galvanized steel, crucial for the longevity of components in infrastructure such as high-speed rail. The study underscores the importance of these coatings for global galvanizing market leadership and calls for improved adhesion and resistance to meet the demands of aggressive environments.

The research compiles innovative approaches and discoveries in the field, spotlighting novel coatings like silane, rare-earth conversion, and conductive polymer films. It also points to the need for evolving existing coating systems to tackle worsening environmental conditions. A significant part of the discussion focuses on the absence of standardized methods for evaluating the lifespan of these coatings, advocating for the development of universal criteria that would significantly impact the industry by allowing for more accurate predictions of coating longevity.

Kania's research in 2020 [21,22] has been pivotal in advancing the zinc coating industry, highlighting the critical importance of cost-effective, high-quality anti-corrosive coatings through optimized batch hot-dip galvanizing processes. The focus has been on minimizing zinc loss and improving the efficiency of steel coating processes. The composition of the galvanizing bath emerges as a significant factor, influencing the steel's reactivity and the overall quality of the zinc coating. Alloying elements such as nickel (Ni) modulate the steel's reactivity, with aluminum (Al) serving as a protector against oxidation. However, this optimization demands careful consideration of the environmental and structural implications of additives such as bismuth (Bi) and tin (Sn), which can pose risks including toxicity and liquid metal embrittlement (LME).

Grandhi, 2021 [23], discusses how to obtain even and good-looking Zn–Mn alloy coatings by solving the issue of uneven colors caused by oxides forming when the steel is pulled from the dipping bath. The key is adding aluminum to the bath to prevent these oxides from forming on the surface. When manganese is added to the mix, especially more than 0.1%, it changes how the coating looks under a microscope, affecting the delta and zeta layers. However, this change does not hurt how well the coating sticks to the steel or its durability.

The study also points out a significant boost in the coating's ability to resist corrosion. The hot-dip Zn–0.2Al–1.2Mn alloy coating was 65% more resistant to rust compared to the usual hot-dip Zn coating. This is because the alloy coating has a better structure at the microscopic level. Tests showed that these Zn–Al–Mn coatings are much better at dealing with corrosion than just plain Zn coatings. Adding Mn also helps control rust buildup, making the coating last longer under harsh conditions like salt sprays. This research suggests that adding certain elements to the coating could make metal protections last longer against corrosion.

Šmak, 2021 [24], explored the impact of hot-dip galvanizing on different grades of high-strength steels and different silicon contents. The study reveals that while DOMEX-type steels with yield strengths up to 700 MPa maintain their mechanical integrity post-galvanization, HARDOX and ARMOX steels exhibit significant decreases in yield and tensile strengths as well as hardness. The deterioration in mechanical properties for

the latter steels is attributed to the tempering of their martensitic structure during the galvanizing process.

The investigation advises that hot-dip galvanizing should be confined to high-strength steels with lower yield strengths, where the process does not markedly alter their mechanical properties. For steel above 700 MPa yield strength, particularly HARDOX and ARMOX, the method is not recommended due to the excessive loss of hardness and strength. This guidance is particularly relevant for industries where the structural integrity of steel components is critical and must be preserved after anti-corrosive treatments.

In this work, meticulous attention has been devoted to the aforementioned observations, underscoring their significance within the broader context of galvanization research. Building upon a foundation of systematic inquiry, this study delves deep into the microstructural intricacies evident during brief temporal intervals. Through rigorous analysis, it becomes palpably clear that the implications of silicon's influence manifest more saliently over extended durations, as opposed to transient phases.

Given these insights, the focus of the study then gravitates towards the formulation of a substantive hypothesis. This posits a distinct mechanism concerning the ingress of the liquid phase, navigated via the interfaces of ζ–ζ boundaries. The hypothesis elucidates that such penetration is governed by nuanced fluctuations in surface free energies. These energy variances, in turn, facilitate the permeation of the liquid phase, all the while adhering to the foundational Gibbs-Smith condition. This proposition offers a holistic perspective, potentially bridging gaps in our current understanding of the intricate interplay between elements during the galvanization process.

## 2. Materials and Methods

### *2.1. Materials*

Two commercial-grade structural steels have been selected: a 4 mm-thick ASTM A36 steel plate and an L-shaped profile of high strength, low-alloy steel-grade Q345B from China's GB/T 1591-2008 standard [25], 6 mm thick and 60 mm wide each.

The materials, A36 and Q345B, were selected based on their reactivity, which is visibly distinct to the naked eye in the galvanizing facility. A36 has low reactivity and a shiny appearance, whereas Q345B has high reactivity and an opaque, mottled appearance. The industrial-sized galvanizing bath has dimensions measuring 7.00 m in length, 1.15 m in width, and 2.00 m in depth. It contains 115,000 kg of molten zinc at a temperature of 443 °C.

The chemical composition of both steels is found in Table 1.

**Table 1.** Chemical composition of steels [1].

| Steel | %C | %Si | %Mn | %P | %S |
|---|---|---|---|---|---|
| ASTM A36 | 0.149 | 0.027 | 0.880 | 0.0217 | 0.0085 |
| Q345B | 0.160 | 0.37 | 1.440 | 0.0270 | 0.0270 |

[1]—Wt %.

The standard pretreatment process for the galvanizing plant consists of an alkaline degreaser, followed by chemical pickling in a 12% hydrochloric acid solution. Afterwards, an $NH_4Cl$ + ZnCl flux is applied, and the pieces are galvanized for durations of 15, 30, and 300 s.

### *2.2. Methods*

The characterization and identification of the phases that make up the microstructure of the galvanized coating samples in all the generated conditions was carried out in laboratories and facilities of the Metallurgical Engineering Department of the University of Santiago de Chile.

The heating curves for both steels were generated using samples: 100 mm × 100 mm × 4 mm plates for A36 and 6 mm thick angles with a length of 100 mm for Q345B. with the

help of a Brainchild VR-18 6-channel data logger with type K thermocouples placed at the center of the plate and the center of the angle wing, as required.

The sample preparation involved the standard assembly using bakelite, followed by grinding, polishing, and chemical etching with nital 3 reagent.

Observations through optical microscopy were carried out using an Olympus metallographic microscope with image acquisition software.

A JEOL JSM-6010LA Scanning Electron Microscope (SEM, JEOL Ltd., Tokyo, Japan), which operates at 20 KV, was used to observe the morphological details of the phases present in the microstructure.

The identification of phases used a Rigaku Diffractometer (Rigaku Americas Corporation, The Woodlands, TX, USA) model Miniflex 600, with the following operating parameters:

- Characteristic radiation of chromium (λ = 2.289750 Å).
- Graphite monochromator-Voltage: 40 kV.
- Current: 30 mA-Converging slit: 1 mm.
- Divergent slit: 1 mm.
- Detector slit: 0.1 mm.
- Sweep range: 40°–140°.
- Time per step: 10 s.
- Angle per step: 0.02°.

Considering that X-ray diffraction has limited penetration depth, XRD was performed initially over the entire coating. Subsequently, the depth of the sample was gradually reduced by paper-sanding it in multiple steps to conduct XRD analysis on progressive layers, thereby enabling us to detect the presence of phases at varying depths within the coating.

## 3. Results

The following section delineates the findings, shedding light on the differences in reactivity between A36 and Q345B steels during galvanization.

### *3.1. Chemical Compositions*

The chemical composition of the zinc bath for galvanizing is found in Table 2.

**Table 2.** Chemical composition of galvanizing bath [1].

| Zinc Bath | %Al | %Pb | %Fe | %Ni | Zn |
|---|---|---|---|---|---|
| Plant 1 | 0.0022 | 0.755 | 0.0239 | 0.0007 | Bal. |

[1]—Wt %.

### *3.2. Heating Curves*

The heating curves are depicted in the graph of Figure 1. In the industrial galvanizing process, the initial temperature of steel is ambient. Thus, it can be determined that there is a period of time in which zinc solidification occurs in the environment of the piece. Given this effect, the contact with the liquid phase delays the time necessary for the piece to reach the melting temperature of zinc, approximately 420 °C, which takes 17 s for the 4 mm plate and 23 s for the 6 mm profile.

### *3.3. Microstructures*

#### 3.3.1. ASTM A36 Low-Silicon Steel Plate

Figure 2 shows the microstructural evolution of the coating phases for low-silicon steel, where it can be observed that Fe-Zn phases are present as early as 5 s, indicating that the reactions begin with zinc in its solid state, as observed by Sepper in 2016 [14].

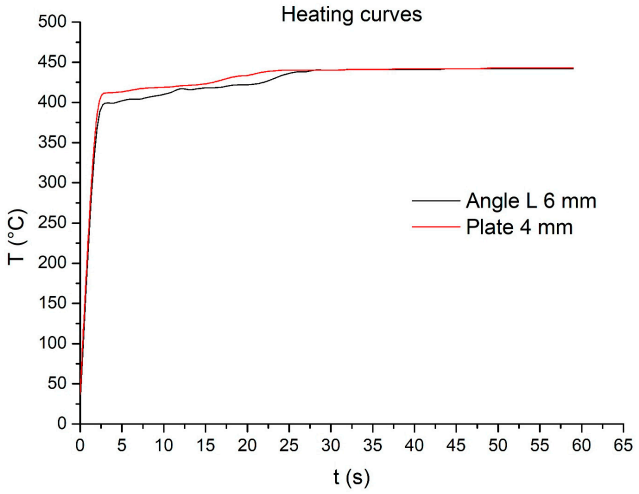



**Figure 1.** Heating curves during galvanizing.

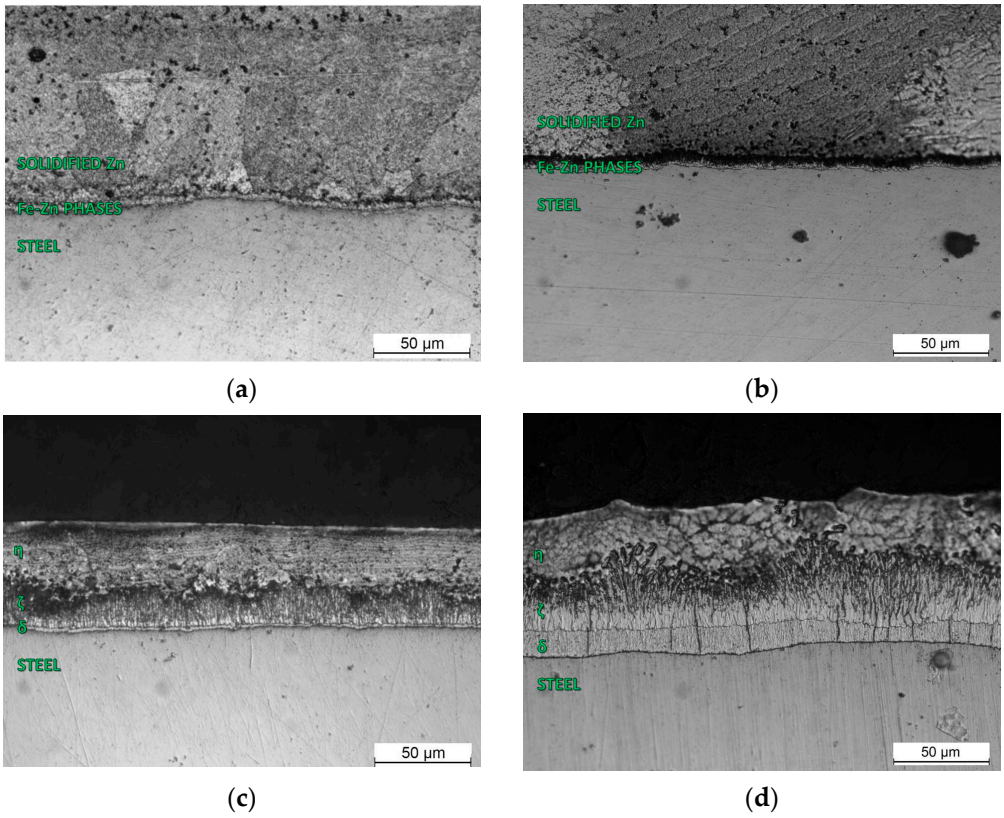



**Figure 2.** Microstructural evolution of galvanized ASTM A36 low-silicon steel: (**a**) 5 s; (**b**) 15 s; (**c**) 30 s; (**d**) 300 s.

With extended exposure times, it is possible to observe that the liquid phase was present and appears as an external layer of solidified zinc. The typical layer morphology of Fe–Zn alloys is evident.

The presence of the Γ phase was not detected using optical microscopy.

### 3.3.2. Q345B High-Silicon Steel Angle

Figure 3 shows the microstructural evolution of the coating for high-silicon steel. Under the same conditions observed at 15 s, similar to low-silicon steel, Fe–Zn phases are present only in solid phases.

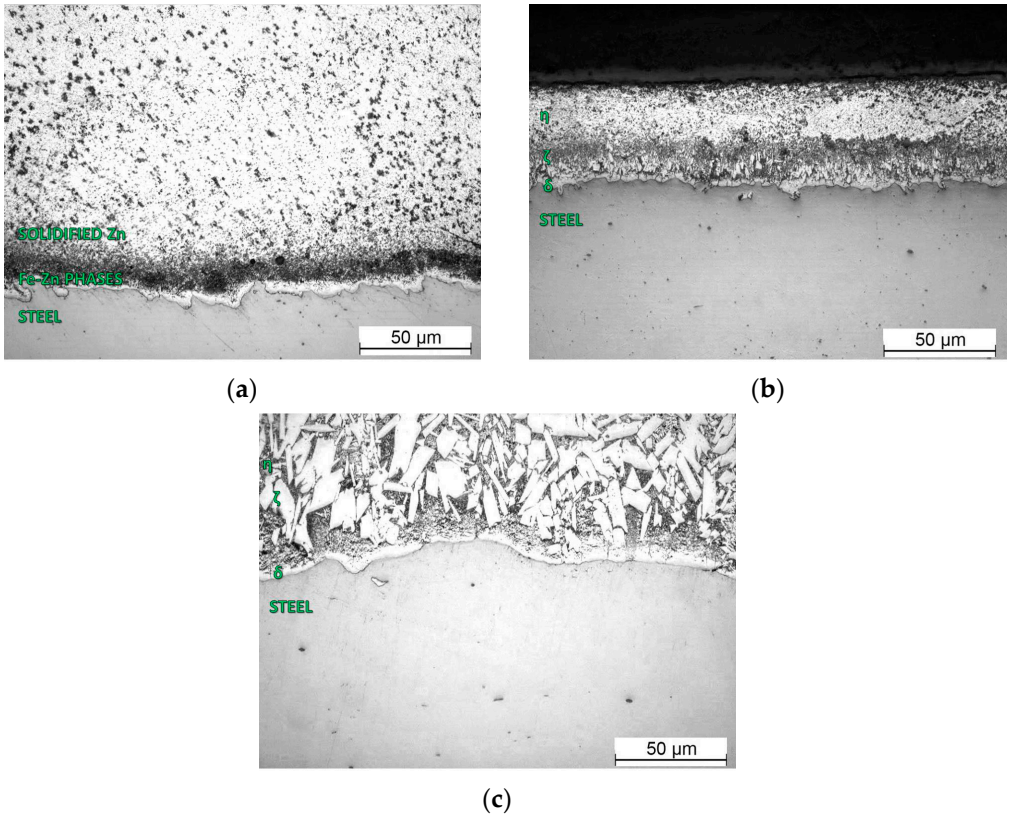



**Figure 3.** Microstructural evolution of galvanized steel Q345B high in silicon: (**a**) 15 s; (**b**) 30 s; (**c**) 300 s.

At intervals of 15 and 30 s, a continuous and compact layer of the ζ phase is visible. Over extended durations, a combination of ζ and η phases is evident on top of a thin layer of the δ phase.

During prolonged periods, the liquid phase penetrates the ζ phase layer via ζ–ζ boundaries, leading to an acceleration in solute transport by the liquid phase and a subsequent increase in reaction rate.

No Γ phase is detected in high-silicon steel, as anticipated in the ternary Fe–Zn–Si system [13].

#### 3.3.3. Phase Identification

SEM/EDS Analysis

The EDS analysis for the 5 s sample of low-silicon steel is presented in Figure 4 and Table 3. Intermetallic compounds are evident, due to the fact that the diffusion coefficient of iron in zinc surpasses that of zinc in iron [14]. Moreover, the saturation of zinc in iron precedes other processes. This is corroborated by the morphological signs pointing to the presence of the ζ phase. However, the composition of this recently formed ζ phase features a higher iron content than its equilibrium counterpart.

**Table 3.** EDS analysis steel/zinc interface in 5 s of reaction, low-silicon steel [1].

| Point | Phase | %Fe | %Zn |
|---|---|---|---|
| 1 | ζ | 13.24 | 86.76 |
| 2 | ζ | 14.8 | 85.2 |
| 3 | α-ζ | 26.29 | 73.71 |

[1]—At%.

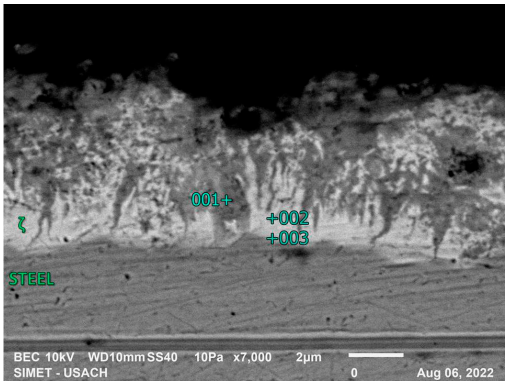



**Figure 4.** Steel/zinc interface analysis in 5 s, low-silicon steel.

For the 15 s sample, in which the zinc remains in its solid state, two phases of the coating are evident in Figure 5. The EDS analysis presented in Table 4 indicates the presence of the δ and ζ phases, and it also shows that the α phase has absorbed zinc.

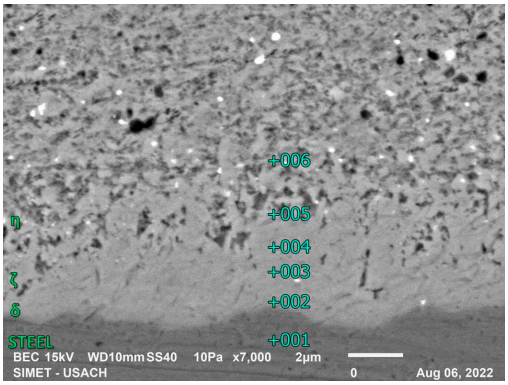



**Figure 5.** Steel/zinc interface analysis in 15 s, low-silicon steel.

**Table 4.** EDS analysis steel/zinc interface in 15 s of reaction, low-silicon steel [1].

| Point | Phase | %Fe | %Zn |
|---|---|---|---|
| 1 | α | 96.41 | 3.59 |
| 2 | δ | 33.85 | 66.15 |
| 3 | ζ | 12.41 | 87.59 |
| 4 | ζ | 10.07 | 89.93 |
| 5 | ζ | 8.3 | 91.7 |
| 6 | η + ζ | 5.32 | 94.68 |

[1]—At%.

Figure 6 and Table 5 present the EDS analysis for the 15 s sample of high-silicon steel. Intermetallic compounds are evident, and the morphology indicates the coexistence of the ζ and δ phases.

**Table 5.** EDS analysis α/δ/ζ/η interface in 15 s, high-silicon steel [1].

| Point | Phase | %Fe | %Zn | %Si |
|---|---|---|---|---|
| 1 | δ | 12.63 | 87.1 | 0.18 |
| 2 | ζ | 9.52 | 90.08 | 0.4 |
| 3 | η + ζ | 3.71 | 95.82 | 0.29 |

[1]—At%.

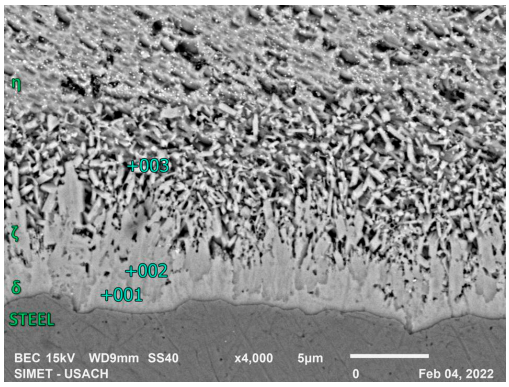



**Figure 6.** $\alpha/\delta/\zeta/\eta$ interface analysis in 15 s, high-silicon steel.

The 300 s galvanization displays the characteristic microstructure of hot-dip galvanized high-silicon steel, as seen in Figure 7. EDS analysis was carried out along lines perpendicular to the ferrous substrate in two zones:

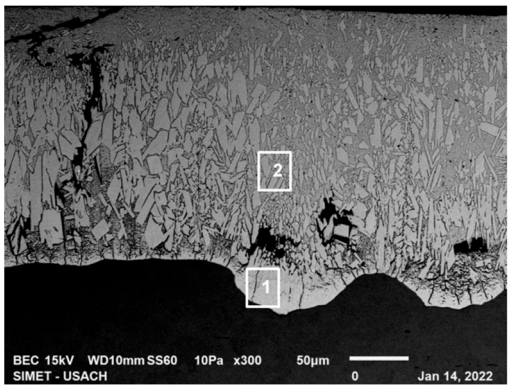



**Figure 7.** 300 s microstructure, high-silicon steel.

Zone 1: $\alpha/\delta/\zeta$ interface, as illustrated in Figure 8 and detailed in Table 6.

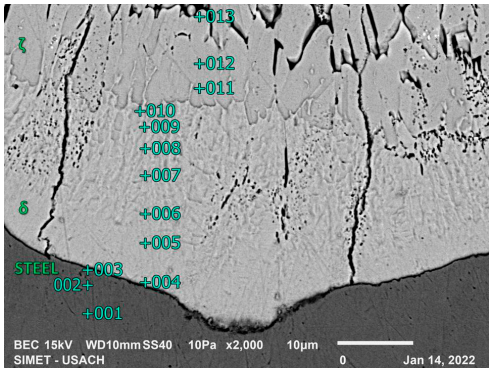



**Figure 8.** $\alpha/\delta/\zeta$ interface analysis in 300 s, high-silicon steel.

Zone 2: $\zeta/\eta$ interface, shown in Figure 9 and described in Table 7.

**Table 6.** EDS analysis α/δ/ζ interface in 300 s, high-silicon steel [1].

| Point | Phase | %Fe | %Zn | %Si |
|---|---|---|---|---|
| 1 | α | 98.23 | 1.21 | 0.56 |
| 2 | α | 97.36 | 2.05 | 0.3 |
| 3 | α | 89.77 | 9.78 | 0.45 |
| 4 | δ | 21.74 | 77.92 | 0.15 |
| 5 | δ | 16.23 | 83.48 | 0.29 |
| 6 | δ | 12.92 | 86.85 | 0.23 |
| 7 | δ | 11.91 | 87.82 | 0.27 |
| 8 | δ | 10.77 | 88.94 | 0.29 |
| 9 | δ | 10.37 | 89.3 | 0.33 |
| 10 | δ | 10.24 | 89.45 | 0.31 |
| 11 | ζ | 9.03 | 90.65 | 0.32 |
| 12 | ζ | 8.91 | 90.76 | 0.14 |
| 13 | ζ | 8.48 | 91.22 | 0.3 |

[1]—At%.

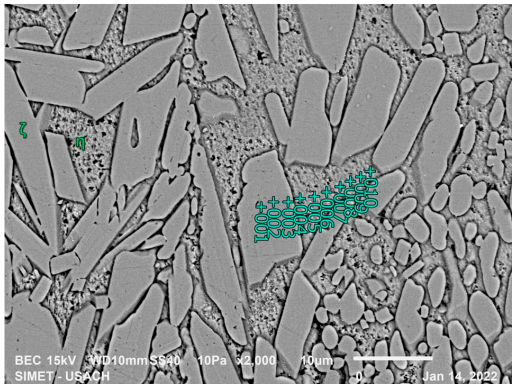



**Figure 9.** ζ/η interface analysis in 300 s, high-silicon steel.

**Table 7.** EDS analysis ζ/η interface in 300 s, high-silicon steel [1].

| Point | Phase | %Fe | %Zn | %Si |
|---|---|---|---|---|
| 1 | ζ | 7.9 | 91.68 | 0.42 |
| 2 | ζ | 7.82 | 91.82 | 0.36 |
| 3 | ζ | 7.88 | 91.81 | 0.31 |
| 4 | η | 1.48 | 97.82 | 0.38 |
| 5 | η | 1.51 | 98.22 | 0.28 |
| 6 | η | 1.48 | 98.29 | 0.22 |
| 7 | η | 1.58 | 98.17 | 0.26 |
| 8 | η | 1.65 | 97.97 | 0.38 |
| 9 | η | 1.57 | 98.11 | 0.32 |
| 10 | η | 1.67 | 97.35 | 0.46 |

[1]—At%.

In the upper side of the coating, the phases are ζ and η with nearly equilibrium compositions. Table 7 shows that at the ζ/η interface, silicon accumulates in the η phase near the ζ phase.

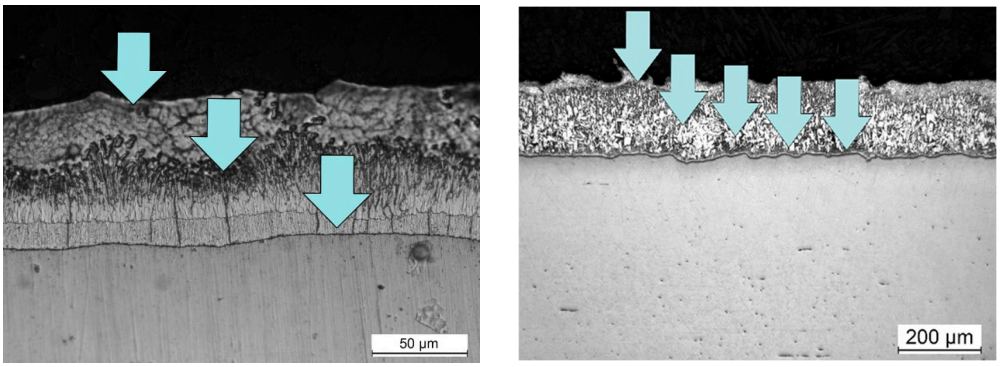
XRD Analysis

The presence of the phases has been verified by X-ray diffraction equipment with a chromium tube (λ = 2.289750 Å) was carried out in multiple stages:

For A36 Steel, the arrows in Figure 10a show the approximate position of the incidence of the X-ray beam after grinding:

1. The X-ray beam is incident on the complete coating, 75 microns.

2. The X-ray beam hits the rough coating at 40 microns.
3. The X-ray beam hits the rough coating at 6 microns.




(**a**) (**b**)

**Figure 10.** XRD test position: (**a**) A36 Steel; (**b**) Q345B steel.

For Q345 Steel, the arrows in Figure 10b show the approximate position of the incidence of the X-ray beam after grinding:

1. The X-ray beam is incident on the complete coating, 180 microns.
2. The X-ray beam hits the rough coating at 80 microns.
3. The X-ray beam hits the rough coating at 60 microns.
4. The X-ray beam hits the rough coating at 40 microns.
5. The X-ray beam hits the rough coating at 20 microns.

In Figure 11, the superimposed diffractograms for the 300 s samples of low-silicon steel are displayed along with the corresponding phase identifications. In the complete coating, the presence of the η(Zn) phase and the ζ phase is evident. As we progress into the depth of the coating, we observe a decrease in the intensity of both the η(Zn) phase and the ζ phase, while the intensity of the δ phase increases. Eventually, the X-ray beam reaches the ferrous substrate, marked by the appearance of the peak corresponding to α.

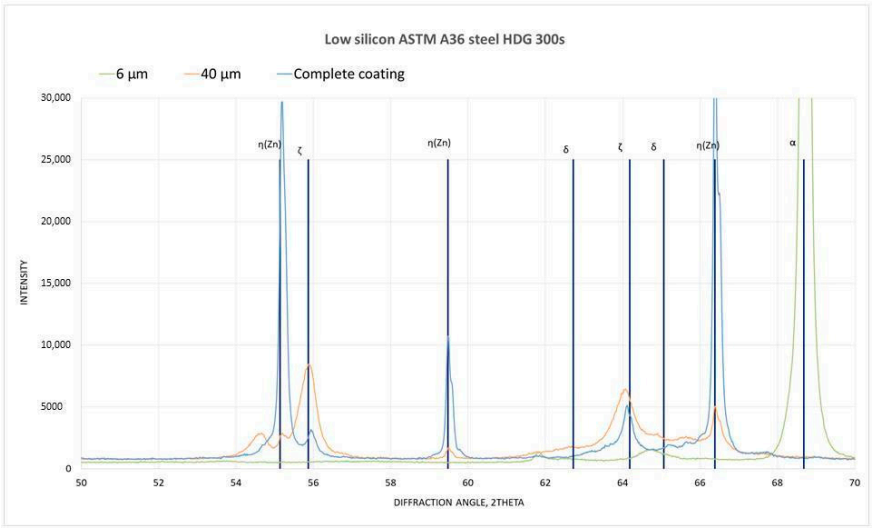



**Figure 11.** Low-silicon steel XRD pattern.

Figure 12 presents the superimposed diffractograms of the 300 s samples of high-silicon steel, along with the corresponding phase identifications. Throughout the coating, both the η(Zn) phase and the ζ phase are consistently present. As we delve deeper into the coating, we notice a slight decrease in the intensity of the η(Zn) and ζ phase peaks,

which aligns with our findings from the metallographic examination. Simultaneously, the intensity of the δ phase increases until it eventually reaches the iron substrate, as evidenced by the appearance of the peak corresponding to ferrite α.

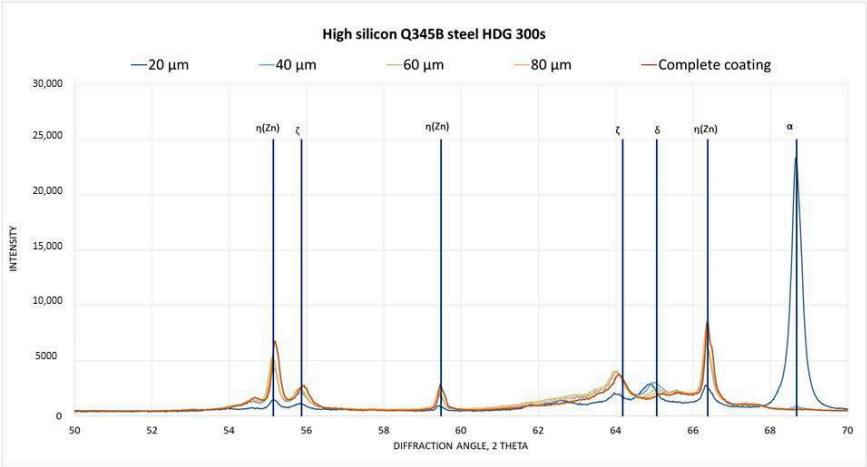



**Figure 12.** High-silicon steel XRD pattern.

The Γ phase is not detected in both steels at the 300 s of galvanization.

## 4. Discussion

The XRD analysis in Figures 11 and 12 reveals that both steels exhibit the same phases—α, δ, ζ, and η. However, the morphology of these phases differs significantly after 5 min of galvanization. As the coating depth is examined, it becomes evident that phases η and ζ gradually decrease and eventually disappear completely, corroborating the state of the coating layers in low-silicon steels. In contrast, high-silicon steels exhibit the persistent presence of ζ and η phases throughout the coating, indicating the existence of a liquid phase in close proximity to the substrate. This liquid phase enhances the mobility and transport of iron atoms, resulting in a highly reactive condition of the steel with molten zinc.

Figures 4–6 depict the initial phase formation in both steels at 5, 15, and 30 s. During these early stages, when only solid phases are present, we observe similarities in the thickness and morphology of the ζ phase. This similarity persists even at 30 s, when a liquid phase is now present. Notably, a continuous ζ phase is observed in both cases. These findings align with Sepper's observations [14], indicating that the effect of silicon is not prominent in the early stages of phase formation. This suggests that the mechanisms responsible for coating formation in high-silicon steels become active in the presence of the liquid phase, which is enriched in silicon at the ζ–liquid interface, as shown in Figure 9 and Table 7. Additionally, as suggested by Kozdras [10], the silicon-enriched liquid may attack the ζ–ζ interface, facilitating the infiltration of the ζ layer.

Images from Figure 7, captured at extended time intervals, reveal the dispersion of the ζ phase within the η phase. From a phenomenological standpoint, it becomes evident that there is a stage where the liquid can efficiently wet a ζ–ζ grain boundary. This phenomenon aligns with the Gibbs-Smith condition [26].

$$\sigma_{gb} > 2\sigma_{ls} \quad (1)$$

The grain boundary free energy (solid–solid interface) for a specific grain boundary must exceed twice the free energy of the solid–liquid interface. As the Fe–Zn phases grow, the surplus silicon in the liquid phase leads to a reduction in the surface energy of the liquid–ζ interface.

## 5. Conclusions

1. The reactions for the formation of layers of Fe–Zn intermetallic compounds in galvanizing on an industrial scale begin during the steel heating stage.
2. The Fe–Zn phase formation sequence in this process is first ζ, then δ; no Γ phase was detected at industrial galvanizing conditions.
3. Due to the layered nature of the coating, it is possible to identify the phases present through X-ray diffraction analysis of samples that have been progressively removed from their coating.
4. The effect of silicon is not observable at times less than 30 s, at which time the liquid phase is already present, and the coating consists of a δ layer followed by a continuous and compact ζ layer covered with liquid.
5. Observations of the ζ/η interface indicate that silicon is driven towards the liquid, accumulating there. This results in an accelerated reaction mechanism, stemming from the alteration of the liquid/ζ interface energy. This shift aligns with the Gibbs-Smith condition, suggesting the infiltration of the liquid phase through the ζ/ζ boundaries, as stated by Kozdras in 1989 [10].

**Author Contributions:** Conceptualization, O.B.; Methodology, C.S. and H.B.; Validation, A.A.; Investigation, C.S.; Resources, O.B. and A.A.; Writing—original draft, C.S.; Writing—review and editing, H.B.; Supervision, O.B. All authors have read and agreed to the published version of the manuscript.

**Funding:** This research was funded by Agencia Nacional de Investigación y Desarrollo, proyecto FONDEF ANID, TDP 210012.

**Data Availability Statement:** The data presented in this study are available on request from the corresponding author. The data are not publicly available due to there's industrial sensitive data.

**Acknowledgments:** The authors would like to thank to Bbosch Galvanizing Company in Chile for supporting us and making their facilities available to us.

**Conflicts of Interest:** The authors declare no conflict of interest.

## References

1. Kania, H.; Saternus, M. Evaluation and Current State of Primary and Secondary Zinc Production—A Review. *Appl. Sci.* **2023**, *13*, 2003. [CrossRef]
2. Xiong, W.; Kong, Y.; Du, Y.; Liu, Z.-K.; Selleby, M.; Sun, W.-H. Thermodynamic Investigation of the Galvanizing Systems, I: Refinement of the Thermodynamic Description for the Fe–Zn System. *Calphad* **2009**, *33*, 433–440. [CrossRef]
3. Petersen, S.; Spencer, P.J.; Hack, K. A Thermodynamic Evaluation of the Iron-Zinc System. *Thermochim. Acta* **1988**, *129*, 77–87. [CrossRef]
4. Han, K.; Ohnuma, I.; Okuda, K.; Kainuma, R. Experimental Determination of Phase Diagram in the Zn-Fe Binary System. *J. Alloys Compd.* **2018**, *737*, 490–504. [CrossRef]
5. Perrot, P.; Dauphin, J.Y. Calculation of the Fe-Zn-Si Phase Diagram between 773 and 1173 K. *Calphad* **1988**, *12*, 33–40. [CrossRef]
6. Marder, A.R. The Metallurgy of Zinc-Coated Steel. *Prog. Mater. Sci.* **2000**, *45*, 191–271. [CrossRef]
7. Pokorny, P.; Kolísko, J.; Balík, L.; Novak, P. Reaction Kinetics of the Formation of Intermetallic Fe–Zn during Hot-Dip Galvanizing of Steel. *Metalurgija* **2016**, *55*, 111–114.
8. Guttmann, M. Diffusive Phase Transformations in Hot Dip Galvanizing. *Mater. Sci. Forum* **1994**, *155–156*, 527–548. [CrossRef]
9. Mackowiak, J.; Short, N.R. Metallurgy of Galvanized Coatings. *Int. Met. Rev.* **1979**, *24*, 1–19. [CrossRef]
10. Kozdras, M.S.; Niessen, P. Silicon-Induced Destabilization of Galvanized Coatings in the Sandelin Peak Region. *Metallography* **1989**, *22*, 253–267. [CrossRef]
11. Foct, J.; Perrot, P.; Reumont, G. Interpretation of the Role of Silicon on the Galvanizing Reaction Based on Kinetics, Morphology and Thermodynamics. *Scr. Metall. Mater.* **1993**, *28*, 1195–1200. [CrossRef]
12. Su, X.; Tang, N.-Y.; Toguri, J.M. 450 °C Isothermal Section of the Fe-Zn-Si Ternary Phase Diagram. *Can. Metall. Q.* **2001**, *40*, 377–384. [CrossRef]
13. Raghavan, V. Ternary and Higher Order Iron Phase Diagram Updates. *J. Phase Equilibria Diffus.* **2010**, *31*, 366. [CrossRef]
14. Sepper, S.; Peetsalu, P.; Kulu, P.; Saarna, M.; Mikli, V. The Role of Silicon in the Hot Dip Galvanizing Process. *Proc. Est. Acad. Sci.* **2016**, *65*, 159. [CrossRef]
15. Bondareva, O.; Melnikov, A. Effect of the Silicon Content in Steel on the Hot-Dip Zinc Coating Microstructure Formation. *IOP Conf. Ser. Mater. Sci. Eng.* **2016**, *156*, 012015. [CrossRef]

16. Che, C.S.; Lu, J.T.; Kong, G.; Xu, Q.Y.; Chen, J.H. Influence of Silicon in Steel on Galvanized Coatings. *Acta Metall. Sin. Engl. Lett.* **2006**, *19*, 85–90. [CrossRef]
17. Gellings, P.J. Mechanism of the Reaction between Liquid Zinc and Steel. *Corros. Sci.* **1974**, *14*, 507–509. [CrossRef]
18. Pokorný, P.; Kolísko, J.; Balík, L.; Novák, P. Effect of Chemical Composition of Steel on the Structure of Hot—Dip Galvanized Coating. *Metalurgija* **2016**, *55*, 115–118.
19. Bondareva, O.S.; Turovsky, A.M.; Turovsky, Y.M. Application of Nickel Tablets in Hot-Dip Galvanizing for Silicon and Phosphorus Steel Reactivity Control. *Mater. Sci. Forum* **2020**, *992*, 689–694. [CrossRef]
20. Yu, Z.; Hu, J.; Meng, H. A Review of Recent Developments in Coating Systems for Hot-Dip Galvanized Steel. *Front. Mater.* **2020**, *7*, 74. [CrossRef]
21. Kania, H.; Saternus, M.; Kudláček, J.; Svoboda, J. Microstructure Characterization and Corrosion Resistance of Zinc Coating Obtained in a Zn-AlNiBi Galvanizing Bath. *Coatings* **2020**, *10*, 758. [CrossRef]
22. Kania, H.; Mendala, J.; Kozuba, J.; Saternus, M. Development of Bath Chemical Composition for Batch Hot-Dip Galvanizing—A Review. *Materials* **2020**, *13*, 4168. [CrossRef]
23. Grandhi, S.; Raja, V.S.; Parida, S. Effect of Manganese Addition on the Appearance, Morphology, and Corrosion Resistance of Hot-Dip Galvanized Zinc Coating. *Surf. Coat. Technol.* **2021**, *421*, 127377. [CrossRef]
24. Šmak, M.; Kubíček, J.; Kala, J.; Podaný, K.; Vaněrek, J. The Influence of Hot-Dip Galvanizing on the Mechanical Properties of High-Strength Steels. *Materials* **2021**, *14*, 5219. [CrossRef]
25. *GB/T 1591*; High Strength Low Alloy Structural Steels. National Standard of the People's Reppublic of China; Standardization Administration of China: Beijing, China, 2008.
26. Volovitch, P.; Protsenko, P.; Skvortsova, Z.; Traskine, V. Grain Boundary Wetting in Polycrystals: 1. Probability of Wetting of Structural Elements. *Colloid J.* **2002**, *64*, 270–273. [CrossRef]

**Disclaimer/Publisher's Note:** The statements, opinions and data contained in all publications are solely those of the individual author(s) and contributor(s) and not of MDPI and/or the editor(s). MDPI and/or the editor(s) disclaim responsibility for any injury to people or property resulting from any ideas, methods, instructions or products referred to in the content.